Gas adsorption on a C_{60} monolayer

R. A. Trasca,[1] M. W. Cole,[2] T. Coffey,[3] and J. Krim[3]
[1]*Institut for Theoretical Chemistry, Technical University Berlin, D-10623 Berlin, Germany*
[2]*Department of Physics, Pennsylvania State University, University Park, Pennsylvania 16802, USA*
[3]*Department of Physics, North Carolina State University, Box 8202, Raleigh, North Carolina 27695, USA*
(Received 25 July 2007; revised manuscript received 24 February 2008; published 14 April 2008)

The adsorption geometry of various gases on top of a C_{60} monolayer is investigated. The potential energy experienced by an adsorbate atom in the vicinity of a C_{60} molecule consists of Lennard-Jones interactions integrated over the spherical surface of the molecule. The adsorption potential exhibits strongly attractive sites which lead to a commensurate phase. The next adsorption sites are assumed on the basis of the symmetries of the triangular C_{60} array. The competition between different adsorption phases is solved by energy minimization. The onset pressure of each phase is computed and compared with experimental data for Kr on top of a C_{60} monolayer.

DOI: 10.1103/PhysRevE.77.041603 PACS number(s): 68.43.−h, 67.25.bh

I. INTRODUCTION

C_{60} molecules, so-called buckyballs, are molecules of nanometer size whose properties are intermediate between those of monatomic molecules and infinite solids. Their curved geometry and attractive potential can accommodate atoms of appropriate sizes either inside or outside; in the latter case, this leads to the formation of multilayer films [1]. Upon adsorption on other substrates, C_{60} molecules form monolayer and multilayer films. Subsequent adsorption of a different species of atoms or molecules (e.g., noble gases) on the C_{60} film yields an unusual system because the large size ($\sim$1 nm diameter) of the C_{60} molecules results in a highly corrugated adsorption potential with an unusually large lattice constant. This results in an interesting sequence of commensurate phases, depending sensitively on the size of the adsorbate. The present paper addresses this problem by evaluating these phases' energetics at zero temperature. These findings of successive commensurate phases are analogous to those found in experiments and simulations of adsorbed phases on carbon nanotube bundles. This similarity is expected because of a similar magnitude of the corrugation potential and its wavelength [2,3].

In Sec. II we describe an adsorption geometry of a gas on a C_{60} monolayer and identify possible phases of adsorption by minimizing the interaction energy within a unit cell. In Sec. III experimental adsorption data are presented and compared with our calculations. Section IV summarizes our work.

II. ADSORPTION GEOMETRY AND ENERGY MINIMIZATION

In this section, we assess the energetics of various commensurate phases of atomic gases adsorbed on a C_{60} monolayer, asking the order of succesive phases' formation as the coexisting vapor pressure P increases. For the case considered here, adsorption on a hexagonal close-packed monolayer of C_{60} molecules, the adsorption potential is derived as a sum (over the surface) of contributions from all C_{60} molecules on the surface. We assume an adsorbed particle interacts with a C_{60} molecule via Lennard-Jones (LJ) interactions of strength ϵ and hard-core diameter σ,

$$\epsilon = \sqrt{\epsilon_{\mathrm{gas}}\epsilon_{\mathrm{C}}},$$

$$\sigma = (\sigma_{\mathrm{gas}} + \sigma_{\mathrm{C}})/2. \tag{1}$$

In computing $V(r)$ the atomicity of the C_{60} molecule is neglected and replaced with a continuous carbon (two-dimensional) surface density θ. The potential energy experienced by the particle at distance r from the center of a C_{60} molecule is obtained by angular integration of the LJ interaction on the surface,

$$V(r) = N_R \epsilon \frac{1}{Rr}\left[\frac{\sigma^{12}}{5}\left(\frac{1}{(r-R)^{10}} - \frac{1}{(r+R)^{10}}\right) - \frac{\sigma^6}{2}\left(\frac{1}{(r-R)^4} - \frac{1}{(r+R)^4}\right)\right], \tag{2}$$

where $N_R = 4\pi\theta R^2$ is the total number of C atoms of the buckyball, $R = 3.55$ Å is the buckyball's radius and $\theta = 0.38$ Å^{-2} is the surface density of the buckyball. This simple approach [1] is conventional in the field of adsorption on fullerenes because (a) we lack more refined descriptions of V and (b) experimental results confirm the adequacy of the simple model [2].

When the adatom resides outside of the spherical surface, it was found that the interaction potential has a minimum at $R_{\mathrm{min}} = R + \sigma$, where $R = 3.55$ Å is the C_{60} molecule radius (distance to the nuclei) and $\sigma = (\sigma_{\mathrm{gas}} + \sigma_{\mathrm{C}})/2$ [1]. Therefore, the adsorption potential above the monolayer exhibits a pattern of very attractive sites located in the threefold coordinated hollows, at distance R_{min} from each of three neighboring buckyballs; this argument neglects the contributions to the potential from second-nearest neighbors, an approximation accurate to within 0.1%. We call these strong-binding sites A and expect that these are the first to be occupied as P increases, resulting in a commensurate ground state of occupied A sites. This argument is obviously valid for adsorbates with sizes much smaller than C_{60} intermolecular distances, so that adsorbate-adsorbate interactions do not influence ap-

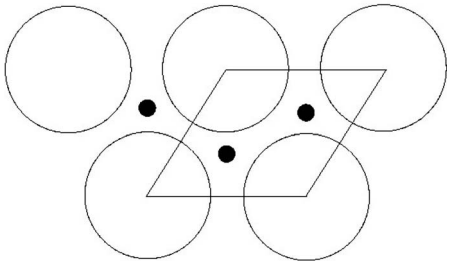

FIG. 1. Cross section through the unit cell of the absorbent (the rhombus) showing the A-type sites (the full circles) on the C_{60} monolayer.

precisely the commensurability of the A phase. A schematic representation of the A phase is shown in Fig. 1.

The geometry of the second adsorbed phase to appear (with increasing pressure) is less obvious than the A phase. We assume that the energy of this phase is minimized when the atoms adsorb on symmetry axes. Figures 2 and 3 show alternative possible adsorbate arrangements, which are discussed below. For either of these phases, the adsorbate-adsorbate interactions play a decisive role in the determination of the potential energy. To assess the energetics, we construct a parallelipiped unit cell whose basis is a rhombus of length equal to the equilibrium separation between two C_{60} molecules, $r_{60}=10.05$ Å. There are two A sites within this cell. As stated above, we assume that the next sites to be occupied (after the A sites) are located somewhere along the symmetry axis between two buckyballs. There arises the possibility of two possible phases: One with three additional atoms in the unit cell, called the B-3 phase (Fig. 2), and one with six more atoms in the unit cell, called the B-6 phase (Fig. 3).

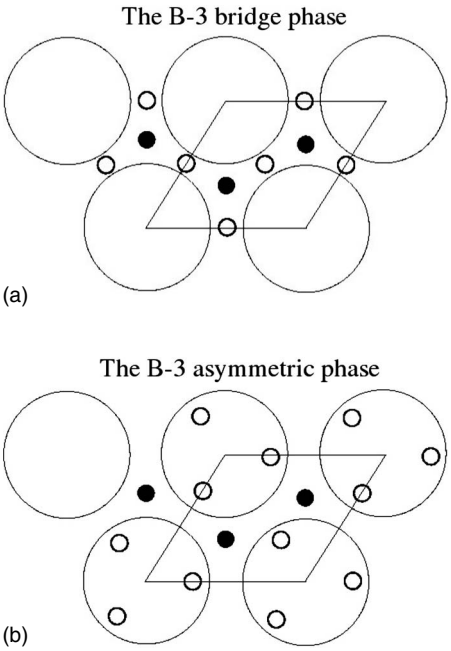

FIG. 2. Schematic depiction of the two possible B-3 phases: (a) The bridge phase and (b) the asymmetric phase. There are three B atoms (empty circles) and two A atoms (full circles) in each unit cell.

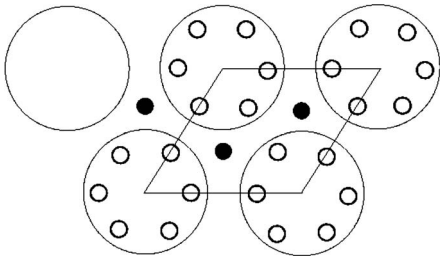

FIG. 3. Schematic depiction of the B-6 phase. There are six B atoms (empty circles) and two A atoms (full circles) in each unit cell.

To find which B phase is energetically preferred, we minimize the energies of the B-3 and B-6 phases in the following way. The position of the B atoms is allowed to vary, but constrained to lie on the symmetry axes. At the same time, the height of the A atoms is varied, since that must change upon adsorption of the B phase. To compute the energy per particle in each phase, we consider the total interaction energy between adatoms in the respective phase, and between adatoms and C_{60} molecules. As a cutoff distance we use the radius of 2 unit cells. At the end we divide the total energy of each phase at the number of adatoms in each phase. The results of the energy minimization are presented schematically in Figs. 2 and 3, and numerically in Table I. As observed in Fig. 2 and Table I, there are two possible configurations of the B-3 phase. For one, called the "bridge phase," the B sites reside at the bridge positions between two buckyballs. For the other "asymmetric phase," the B sites are displaced from the bridge positions. The numerical results of the energy minimization shown in Table I indicate that the B-3 phase is preferred to the B-6 phase for all gases investigated here. The difference between the various gases is that some of them (He, Ne, H_2) exhibit the B-3 bridge phase, while others (Ar, Kr, Xe) exhibit the B-3 asymmetric phase. This difference is a consequence of the adsorbate-adsorbate interaction; adatoms with relatively small sizes and weak interactions localize in the bridge sites, while the larger adatoms minimize their energy by occupying the asymmetric sites.

III. COMPARISON WITH EXPERIMENTS

Comparison between theoretical and experimental data involves knowledge of the thermodynamic quantities. The pressure of the adsorbed film is monitored in the experimental isobars. In theoretical calculations, the pressure is related to the chemical potential of each system. Thus, we employ the thermodynamic equilibrium condition between the adsorbed monolayer and the external gas, equivalence of chemical potentials,

$$\mu_{\text{gas}} = \mu_{\text{film}} \tag{3}$$

where the chemical potential of the gas phase is taken to be that of an ideal classical gas, $\mu_{\text{gas}}=k_BT\ln(P\lambda^3/k_BT)$, T is the temperature and $\lambda=\sqrt{2\pi\hbar^2/(mk_BT)}$ is the de Broglie wavelength. Thus, the pressure of the adsorbed film is

TABLE I. Geometrical and energetic parameters of A, B-3, and B-6 phases for various gases. The meaning of symbols is h_A and h_B are the heights of A and B adatoms above $z=0$ plane, r_{ab} is the nearest-neighbor distance between A and B atoms, r_{bb} is the nearest-neighbor distance between B-type adatoms, E is the energy per particle in each phase.

Phase		He	Ne	H_2	Ar	Kr	Xe
A phase	h_A(Å)	2.9	3.1	3.4	3.8	3.9	4.4
	E_A (K)	−353	−695	−766	-151×10^1	-192×10^1	-253×10^1
B-3 phase	h_A(Å)	3	3.1	3.3	3.6	3.8	4.3
	h_B(Å)	4.1	4.3	4.6	5.5	6	6.8
	r_{ab}(Å)	3.1	3.1	3.1	3.5	3.8	4.5
	r_{ab}(Å)	5.0	5.0	5.0	7.4	6.4	4.6
	E_B (K)	−299	−612	−660	-120×10^1	-151×10^1	-205×10^1
B-6 phase	h_A(Å)	3.0	3.2	3.5	3.9	3.9	
	h_B(Å)	5.3	5.5	5.8	6.0	6.1	
	r_{ab}(Å)	3.9	4.0	4.0	3.9	4.0	
	r_{bb}(Å)	3.7	3.5	3.4	3.4	3.4	
	E_B (K)	−210	−444	−509	−999	−742	

$$P = \exp(\mu_{\text{film}}/k_BT)k_BT/\lambda^3. \quad (4)$$

We are especially interested in identifying the onset point for the various adsorbed phases. The chemical potential at $T=0$ corresponding to the onset can be found from

$$\mu = \frac{\partial E}{\partial N} \approx \frac{E_1 - E_2}{N_1 - N_2}, \quad (5)$$

where subscripts 1,2 correspond to two consecutive phases (e.g., A and B-3). We consider experimental data for adsorption of Kr on top of C_{60} monolayers deposited on Ag(111). To assess the contribution from Ag(111), we estimate the interaction energy between Kr adatoms and Ag(111) surface in each phase using the asymptotic form of the van der Waals interaction $V_{\text{Ag}}(d)=-C/d^3$, where d is the distance between a Kr adatom and the image plane edge of the Ag(111) surface, and C is the Kr-Ag(111) van der Waals coefficient set equal to 2263 meV/K [4]. The distance between the Ag(111) surface and the plane containing the C_{60} centers is taken as 5.8 Å [5]. The contribution of Ag(111) surface to the interaction energy gives only 1%–2% increase to the energy per particle of Kr adatoms in each phase calculated in Table I. Therefore, we consider this contribution negligible. The onset chemical potentials and pressures associated with transitions between the phases introduced in Sec. II are presented in Table II.

A comparison with experiments can be done in the case of Kr, where experiments have been conducted employing a quartz crystal microbalance (QCM) technique. QCM has proven to be a sensitive probe for detecting monolayer adsorbate films and measuring their properties [6–9]. Here, we present measurements of krypton films adsorbing on C_{60} monolayer and bilayer, that were deposited onto Ag(111) surface electrodes of a QCM. Overtone-polished 8 MHz AT (transverse shear) cut quartz crystals were employed for these studies, whose quality factors were near 10^5. The substrates were prepared in ultrahigh vacuum; the base pressure of the vacuum system ranged from 8×10^{-11} to 5×10^{-10} Torr. Thermal evaporation was used to deposit 80 nm of 99.999% pure Ag atop the blank QCM, producing a mosaic structure with a (111) fiber texture [10].

C_{60} substrates were prepared by thermally evaporating C_{60} monolayers atop an 80-nm-thick Ag(111) electrode on a blank QCM. Thermally evaporated C_{60} molecules are known to be quite mobile on Ag(111) surfaces [11], forming well-ordered $2\sqrt{3}\times2\sqrt{3}R30°$ structures [12]. By carefully monitoring the number per unit of C_{60} molecules deposited on the surface, it is therefore possible to form a well ordered and flat layer by stopping deposition at a monolayer coverage.

TABLE II. Thermodynamic parameters of A, B-3, and B-6 phases for various gases. The meaning of symbols is μ is the chemical potential and P is the onset pressure of each phase at 77.4 K.

Phase		He	Ne	H_2	Ar	Kr	Xe
A phase	μ_A (K)	−353	−695	−766	-151×10^1	-192×10^1	-253×10^1
	P_A (torr)	866×10^2	116×10^2	148	0.8	0.01	1.2×10^{-5}
B-3 phase	μ_B (K)	−264	−557	−590	−998	-124×10^1	-174×10^1
	P_B (torr)	27.4×10^4	69.7×10^3	14.3×10^2	660	77.0	2.5×10^{-1}
B-6 phase	μ_B (K)	−163	−360	−424	−826	−349	
	P_B (torr)	10.1×10^5	88.6×10^4	12.2×10^3	61.0×10^2	86.0×10^5	

Since the QCM was operational in the course of the C_{60} deposition, coverage amounts were carefully monitored. The C_{60} was deposited *in-situ* and immediately after the Ag(111) deposition. Data are presented here for Kr uptake on one monolayer (frequency shift of $21+/-1$ Hz; $73+/-4$ ng/cm^2) and two monolayers of C_{60} evaporated onto a Ag(111) electrode. While prior literature has well-documented the in-plane ordering and flatness of the C_{60} monolayer atop Ag(111), the bilayer is less well documented. Our adsorption data presented here do not exhibit any significant increase in out-of-plane roughness or porosity for the bilayer, as would be evidenced by substantially greater uptake [13]. The bilayer appears to be less well-ordered in-plane, however, as evidenced by friction and slip-time measurements recorded on these samples at the two-dimensional solid-liquid transition for these samples [14,15].

After the C_{60} deposition, all samples were immediately transferred *in-situ* to the adsorption cell where they were electrically connected to an external Pierce oscillator circuit. They were then chilled to 77.4 K by submersion in a liquid nitrogen bath. After the samples had come to thermal equilibrium, they were exposed to research grade krypton gas, and frequency shifts were monitored as a function of increasing pressure. [Research grade krypton (99.999% pure) was purchased from Airco Industrial Gases.] The frequency shifts δf are proportional to the mass per unit area of the film that tracks the QCM motion [16]. Film slippage results in some fraction of the mass of the film decoupling from the oscillation of the substrate, and a concomitant reduction in the frequency shift [17].

$$\frac{\delta f_{\text{mass loading}}}{f} = -\frac{2\rho_f t_f}{\rho_q t_q},$$

$$\delta f_{\text{film}} = \frac{\delta f_{\text{mass loading}}}{1+(\omega\tau)^2}. \tag{6}$$

Here, ρ_f and t_f are the density and thickness of the adsorbed film, and ρ_q (2.65 g/cm^3) and t_q (0.021 cm for $f=8$ MHz) are the density and thickness of the QCM. Frequency shifts can also be caused by gas pressure, tensile stress, and temperature, however these effects were negligible in this experiment.

The frequency shift and coverage data for two representative data sets for krypton adsorbing on monolayer and bilayer of C_{60} are shown in Figs. 4(a) and 4(b), respectively. The features present in the monolayer are attributable to better in-plane ordering and the slight differences in the overall frequency shift for the two sets are attributable to differences in slippage and coupling with the substrate [14]. Features are present in the isotherms at coverage's of approximately 0.025, 0.065, and 0.08 atoms/Å^2. At 77.4 K, krypton first forms a liquid monolayer with a coverage of 0.066 atoms/Å^2 ($\approx$26.6 Hz for $f_o=8$ MHz crystals). As the coverage increases, the krypton monolayer becomes more tightly packed and changes phase to a solid, with a monolayer coverage of 0.078 atoms/Å$^2 \approx$ 31.4 Hz [18,19]. We therefore identify the latter two features to correspond to condensation of liquid and solid incommensurate monolayer phases, as has been routinely observed in the past for adsorption on the metal (111) substrates. The feature present in the data set at the coverage of approximately 0.025 atoms/Å^2 and between 0.01 and 0.02 torr is consistent with the presence of the phase A commensurate solid.

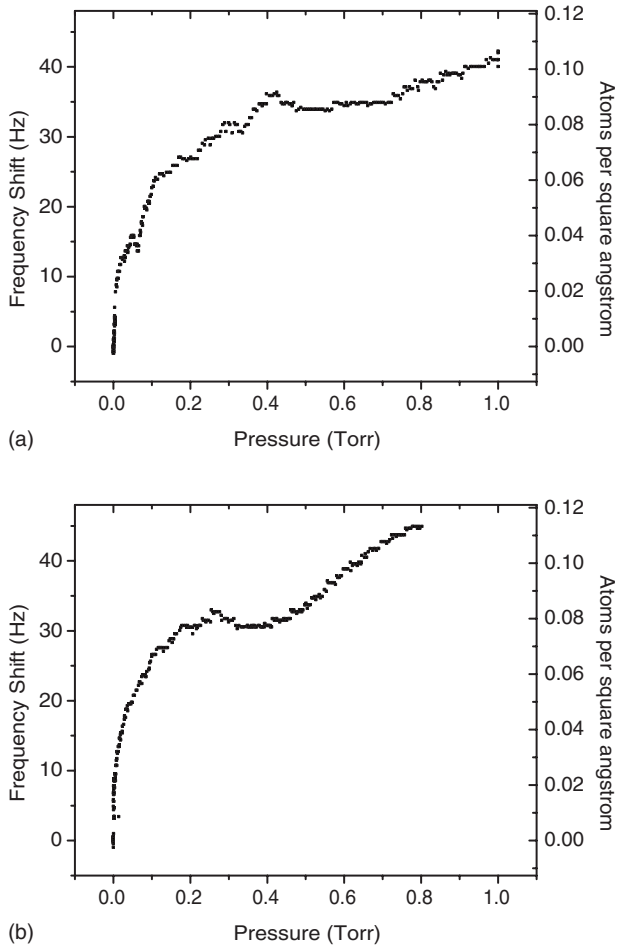

FIG. 4. Frequency shift and coverage data for Kr on (a) monolayer C_{60} and (b) bilayer C_{60}. The slight drop in the data close to 30 Hz is attributable to a change in coupling of the layer associated with the solid-liquid transition. See text and also Ref. [14].

IV. CONCLUSIONS

In conclusion, we have investigated the adsorption of rare gases on a C_{60} monolayer. On the basis of symmetry arguments, we proposed several adsorption geometries. The competition between various phases was solved by energy minimization. The interaction energy was computed as a sum of Lennard-Jones energies and included both adsorbate-substrate as well as adsorbate-adsorbate interactions. Two phases, called A and B, were found corresponding to the first two layers of adsorbed gas. Phase A was localized directly above the hollows between three C_{60} molecules, and phase B was localized directly above or in the vicinity of the bridges between two C_{60} molecules, as shown in Figs. 1 and 2.

Thermodynamic properties of the adsorbed films were also investigated and compared with experimental data. The

onset pressure of various adsorption phases was found using the thermodynamic equilibrium condition between the adsorbed monolayer and the external gas. Adsorption of Kr films on C_{60} monolayer substrates was measured experimentally using the quartz crystal microbalance technique. Frequency shifts proportional with the mass per unit area of the adsorbed film, were monitored as a function of increasing pressure as shown in Figs. 4(a) and 4(b).

Our theoretical calculations of the onset pressure described at the beginning of this section yield a pressure of 0.01 torr for phase A and 77.04 torr for phase B. We identify phase A as the first feature in the experimentally observed isotherm, and incommensurate liquid and solid phases as the next two features. Phase B does not appear to be present in this system. We note however that the theoretically predicted condensation pressure for phase B of 77 torr is substantially higher than the bulk condensation pressure of Kr at 77.4 K, so it appears to be energetically unfavorable with respect to the formation of both incommensurate monolayers and bulk Kr at 77.4 K.

ACKNOWLEDGMENTS

This work has been supported in part by the NSF Grant Nos. DMR0320743 SR, F49620014-0132, and DMR-0505160.

[1] E. S. Hernandez, M. W. Cole, and M. Boninsegni, Phys. Rev. B **68**, 125418 (2003).
[2] See articles in A. D. Migone, Silvina M. Gatica, Mary J. Bojan, Milton W. Cole, M. Mercedes Calbi, and J. Karl Johnson, in *Adsorption by carbons*, edited by J. M. D. Tascon (Elsevier, Holland, in press).
[3] M. M. Calbi, S. M. Gatica, and M. W. Cole, Phys. Rev. B **67**, 205417 (2003).
[4] G. Vidali, G. Ihm, H.-Y. Kim, and M. W. Cole, Surf. Sci. Rep. **12**, 135 (1991).
[5] S. M. Gatica, H. I. Li, R. A. Trasca, M. W. Cole, and R. D. Diehl, Phys. Rev. B **77**, 045414 (2008).
[6] *Applications of Piezoelectric Quartz Crystal Microbalances*, edited by C. Lu and A. Czanderna (Elsevier, Amsterdam, 1984).
[7] W. G. Cady, *Piezoelectricity*, 2nd ed. (Dover, New York, 1964).
[8] D. Salt, *Hy-Q Handbook of quartz crystal devices* (Van Nostrand Reinhold, United Kingdom, in press).
[9] E. T. Watts, J. Krim, and A. Widom, Phys. Rev. B **41**, 3466 (1990).
[10] K. K. Kakati and H. Wilman, J. Phys. D **6**, 1307 (1973).
[11] K. Ait-Mansour, P. Ruffieux, X. Xiao, R. Fasel, P. Groning, and O. Groning, Inst. Phys. Conf. Ser. **61**, 16 (2007).
[12] C. A. Mirkin and W. Brett Calwell, Tetrahedron **52**, 5113 (1996).
[13] C. L. Wang, J. Krim, and M. F. Toney, J. Vac. Sci. Technol. A **7**, 2481 (1989).
[14] T. Coffey and J. Krim, Phys. Rev. B **72**, 235414 (2005).
[15] G. Palasantzas and J. Krim, Phys. Rev. Lett. **73**, 3564 (1994).
[16] G. Z. Sauerbrey, Phys. Verh. **8**, 113 (1957).
[17] M. Chester, L. C. Yang, and J. G. Stephens, Phys. Rev. Lett. **29**, 211 (1972).
[18] J. Krim, J. G. Dash, and J. Suzanne, Phys. Rev. Lett. **52**, 640 (1984).
[19] A. Thomy and X. Duval, in *Adsorption at the Gas-Solid and Liquid-Solid Interface*, edited by J. Rouquerol and K. S. W. Sing (Elsevier, Amsterdam, 1982).